Global Environmental Change 88 (2024) 102917

Contents lists available at ScienceDirect

Global Environmental Change

journal homepage: www.elsevier.com/locate/gloenvcha

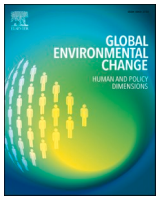

# Floating objects in the open ocean: Unveiling modifications of the pelagic habitat induced by forest cover change and climate variations

Amaël Dupaix [a,*], Matthieu Lengaigne [a], Marco Andrello [b], Nicolas Barrier [a], Laurent Dagorn [a], Quentin Gusmai [c], Gaëlle Viennois [c], Manuela Capello [a]

[a] MARBEC, Univ. Montpellier, CNRS, Ifremer, INRAE, IRD, Sete, France
[b] Institute for the Study of Anthropic Impacts and Sustainability in the Marine Environment, Italian National Research Council (CNR-IAS), Rome, Italy
[c] AMAP, Univ. Montpellier, CIRAD, CNRS, INRAE, IRD, Montpellier, France

ARTICLE INFO

*Keywords:*
Drifting fish aggregating device
Lagrangian simulation
Tropical tuna
Anthropogenic impacts

ABSTRACT

Natural floating objects (NLOGs) are a major component of the habitat of pelagic species. Since the 1990s, the number of floating objects in the open ocean has increased greatly as a result of the introduction of drifting fish aggregating devices (DFADs) by the industrial tropical tuna purse seine vessels. These changes, and their potential impacts on the species that associate with floating objects, remain poorly understood. If the habitat modifications induced by DFADs have been recently characterized and quantified, the impact of other human activities on the number of floating objects is poorly studied. Relying on lagrangian simulations at the scale of the whole Indian Ocean, from 2000 to 2019, we assess the potential modifications of the pelagic surface habitat that could originate from forest cover change and climate variations. We develop several scenarios, based on coastal and river forest cover, precipitations and river discharge, to simulate densities of NLOGs. Our results suggest no significant increase in average NLOG densities in the ocean and highlight important regional and seasonal variations of these densities driven by both forest cover change and precipitations. These preliminary findings underscore the limited understanding of this critical element of pelagic species habitat. Therefore, there is pressing need to intensify monitoring efforts for pelagic species habitat and raise awareness about potential impacts of habitat modifications on tuna and other pelagic species.

## 1. Introduction

In the context of global change, ocean biodiversity is facing degradation due to several direct and indirect drivers (IPBES, 2019). Among these, the exploitation of fish and seafood by fisheries stands as the foremost direct driver, imposing largest impacts (IPBES, 2019). The consequences of increased fishing activities extend beyond mere depletion of marine resources; they also trigger indirect impacts by altering natural habitats (Neumann et al., 2016; IPBES, 2018). For example, research has shown that fishing activities influence the functional composition of benthic species communities (Neumann et al., 2016; Dupaix et al., 2021b) and modify pelagic species habitat (Dupaix et al., 2021a). These habitat modifications, in turn, can substantially affect marine species in terms of distribution, reproduction, behavior and ultimately their fitness (Macura et al., 2019). Consequently, it becomes crucial to understand and assess the scale of these habitat modifications, which result either from global change or direct exploitation of animals.

Numerous pelagic species, including tropical tuna, manifest a well-known association with floating objects (FOBs, Fréon and Dagorn, 2000; Castro et al., 2002). Originally, FOBs were primarily natural debris like parts of trees floating out in the oceans (designated as NLOGs). Fishers have exploited the associative behavior of pelagic species for centuries to aid in their search and catch. Oppian, a Greek poet, detailed in his poem *Halieutica* written in the 2nd century, how fishers use ship wrecks to facilitate the catch of dolphinfish (*Coryphaena hippurus*; Oppian, 1963). Historical evidence also points to the use of anchored fish aggregating devices (AFADs) - *i.e.* man-made objects, moored in coastal areas, to attract targeted fish species. Artisanal fishers in the Mediterranean were deploying AFADs as early as in the 14th century (Taquet, 2013), while a similar practice was observed in Japan during the 17th century (Nakamae, 1991). In more recent times, industrial tuna purse seine vessels introduced drifting fish aggregating devices (DFADs; Davies et al., 2014) in the 1980s. The deployment of

* Corresponding author.
*E-mail address:* amael.dupaix@ens-lyon.fr (A. Dupaix).

https://doi.org/10.1016/j.gloenvcha.2024.102917
Received 18 January 2024; Received in revised form 21 August 2024; Accepted 27 August 2024
Available online 5 September 2024

DFADs has surged over the years, with most recent global estimates ranging from 81,000 to 121,000 deployments yearly (Gershman et al., 2015). Specifically, in the Indian Ocean (IO), Maufroy et al. (2017) reported a fourfold increase in the use of DFADs from 2007 to 2013.

The rising number of FOBs in the open ocean related to the increasing use of DFADs has led to various ecological impacts on tropical tuna populations (Dagorn et al., 2013b; Capello et al., 2023; Pons et al., 2023). Firstly, the presence of DFADs reduces the search effort required by purse seiners, significantly increasing tuna catchability and consequently their fishing mortality (Wain et al., 2021; Song and Shen, 2022). Secondly, fishing on DFADs results in the catch of smaller yellowfin (YFT, *Thunnus albacares*) and bigeye (BET, *T. obsesus*) tuna compared to targeting them in free-swimming schools (not associated with FOBs; IOTC, 2022d; Merino et al., 2020). Within the IO, YFT and BET, two out of the three tropical tuna targeted by purse seiners, are currently facing challenges of overfishing (IOTC, 2022b; IOTC, 2022a). This means that their spawning biomass is below the spawning biomass reference point for maximum sustainable yield. Purse seine vessels account for 34 % of the yearly catch of YFT and 42 % of BET in the IO (IOTC, 2022b; IOTC, 2022a). Consequently, the management of these fisheries necessitates careful consideration of the two aforementioned impacts caused by drifting fish aggregating devices (DFADs).

Beyond the direct effects of increasing fishing mortality, DFADs have the potential to induce indirect ecological impacts on tunas by modifying tuna surface habitat. Evidence indicates that tuna caught in association with FOBs exhibit lower body condition compared to those caught in free-swimming schools (Hallier and Gaertner, 2008; Marsac et al., 2000; Robert et al., 2014). Furthermore, changes in FOBs density may disturb the large-scale movements of tuna, leading to individuals being retained or transported to ecologically unsuitable areas (Marsac et al., 2000; Fonteneau et al., 2013; Schaefer et al., 2015), and potentially influencing tuna schooling behaviour (Capello et al., 2022; Sempo et al., 2013). While scientific consensus on the extent of indirect impacts of DFADs on tuna behaviour and life-history parameters (*e.g.* physiological condition, reproduction; Dupaix et al., 2024) is yet to be reached, these potential impacts emphasize the need to characterize pelagic surface habitat modifications induced by human activities. A recent study (Dupaix et al., 2021a) focused on the Western IO (WIO) and provided insights into the modifications of the pelagic habitat induced by DFADs. By analyzing data from observers onboard purse seine vessels, they revealed a strong increase in the total number of FOBs from 2006 to 2018. The entire WIO was impacted: in recent years, DFADs represent over 85 % of the total number of FOBs and the number of FOB observations per day increased fivefold between 2006 and 2018. To assess these modifications, Dupaix et al. (2021a) took the number of observed NLOGs in the WIO as a reference state, representing conditions unaltered by human activities.

The number of NLOGs, mainly composed of tree parts transported by surface currents, could also be significantly affected by human activities, such as forest cover change, and climate variations which can impact oceanic currents (Krajick, 2001; Thiel and Gutow, 2005; Russell et al., 2014). Deforestation, involving the human-induced conversion of forested land into non-forested land, is mainly driven by agriculture and logging (IPBES, 2018). Since 2000, global logging, for materials, construction and energy production, has seen a substantial increase, with 20% of tropical forests experiencing selective logging (IPBES, 2022). In tropical areas, forested land has decreased in recent decades with tropical forest loss estimated to be approximately 10 million hectares per year, with 60 to 90 % attributed to agriculture (Pendrill et al., 2022). The number of NLOGs can also exhibit strong seasonal and inter-annual variations, influenced by factors like precipitations, modifications in surface currents, and extreme climatic events impacting the release and circulation of NLOGs from sources like rivers and coastal forests (Caddy and Majkowski, 1996; Hinojosa et al., 2011). For example, in Taiwan, the Morakot typhoon in 2009 led to the release of over three million trees into the sea Doong et al. (2011).

In the absence of trajectory and/or position data of NLOGs across the entire ocean, employing Lagrangian simulation models with virtual NLOGs becomes valuable in estimating their distribution. Lagrangian simulations are increasingly being used at ocean basin and global scales to characterize the transport of debris, and the dispersal of fish larvae and plant propagules (Andrello et al., 2017; Van Sebille et al., 2018; Van der Stocken et al., 2019; Fontoura et al., 2022). NLOGs are most likely sourced from river basins or coastal forests (Thiel and Gutow, 2005; Doong et al., 2011), and previous studies have indicated that FOBs drift in a manner similar to oceanic drifters (Imzilen et al., 2019). NLOG's drift can thus predominantly be attributed to surface oceanic currents. This study focuses on characterizing the natural surface habitat of tropical tuna in the IO, specifically determining how the density and distributions of NLOGs has changed between 2000 and 2019, potentially revealing the effects of human activities, such as deforestation, and changes in oceanic circulation linked to climate variations. Given the absence of precise estimations of NLOG distribution in the IO, we aim to (1) describe the distribution of NLOGs and their seasonal variations at the scale of the entire oceanic basin and (2) assess any potential trends in NLOG numbers, which could be linked to deforestation or surface currents' variations.

## 2. Material and methods

### 2.1. Lagrangian simulations

Lagrangian simulations were performed from 2000 to 2019 to simulate the distribution of NLOGs in the Indian Ocean (IO) using the Ichthyop computational tool *v3.3.12* (Lett et al., 2008; Barrier et al., 2023). The delimitation of IO considered in this study is framed in Fig. 1. This tool allows to account for advection–diffusion processes affecting the dispersion of particles (NLOGs in this case) released in a given location of the ocean based on ocean currents. Surface currents were extracted from an eddy-resolving (1/12°) simulation performed using NEMO Ocean General Circulation Model (Madec, 2016) in the framework of the OceaniC Chaos - ImPacts strUcture predicTability (OCCIPUT) project (https://meom-group.github.io/projects/occiput; Penduff et al., 2014; Bessières et al., 2017). The hydrodynamic simulations were driven by the 3-hourly fully-varying atmospheric forcing (the DFS5.2 oceanic forcing product, derived from the ERA-I re-analysis; Dussin et al., 2016). Other simulation settings relevant for this study include release location (Davies et al., 2017; Curnick et al., 2021), release time (Siegel et al., 2003; Curnick et al., 2021) and NLOG lifetime (Pineda et al., 2007; Huret et al., 2010; Van der Stocken et al., 2019). A total of 6,408 cells (1/12° × 1/12°) were identified as coastal cells, defined as cells whose centers lie within 1/12° distance from the coastline. The coastline data was obtained from the IHO (International Hydrographic Organization) coastline shapefile v3 (Institute, 2018), covering a total area of 67 million km$^2$. To have a holistic view of all the potential trajectories, $n = 1000$ particles were released every week within each coastal cell, corresponding to a total of 6.7 billion particles simulated. Particles were advected using NEMO surface currents. Particles were considered stranded and were removed from the simulation when they entered a land cell. Particle densities were then saved as a 2D array every 7 days for each release location and date.

The lifetime of NLOGs, dependent on wood property and on its susceptibility to destruction by secondary consumers, remains poorly known and can range from a few days to up to several years (Thiel and Gutow, 2005). However, past simulations with lifetimes varying from 30 days to a year, revealed that the results were relatively insensitive to lifetime in the IO (Dupaix et al., 2021a). In the current study, an average NLOG lifetime of one year was considered. To this end, particles were transported for a fixed duration of 500 days. The average drifting time of one year was then derived by multiplying the 2D arrays by the probability mass function of an inverse Poisson distribution with $\lambda = 360$

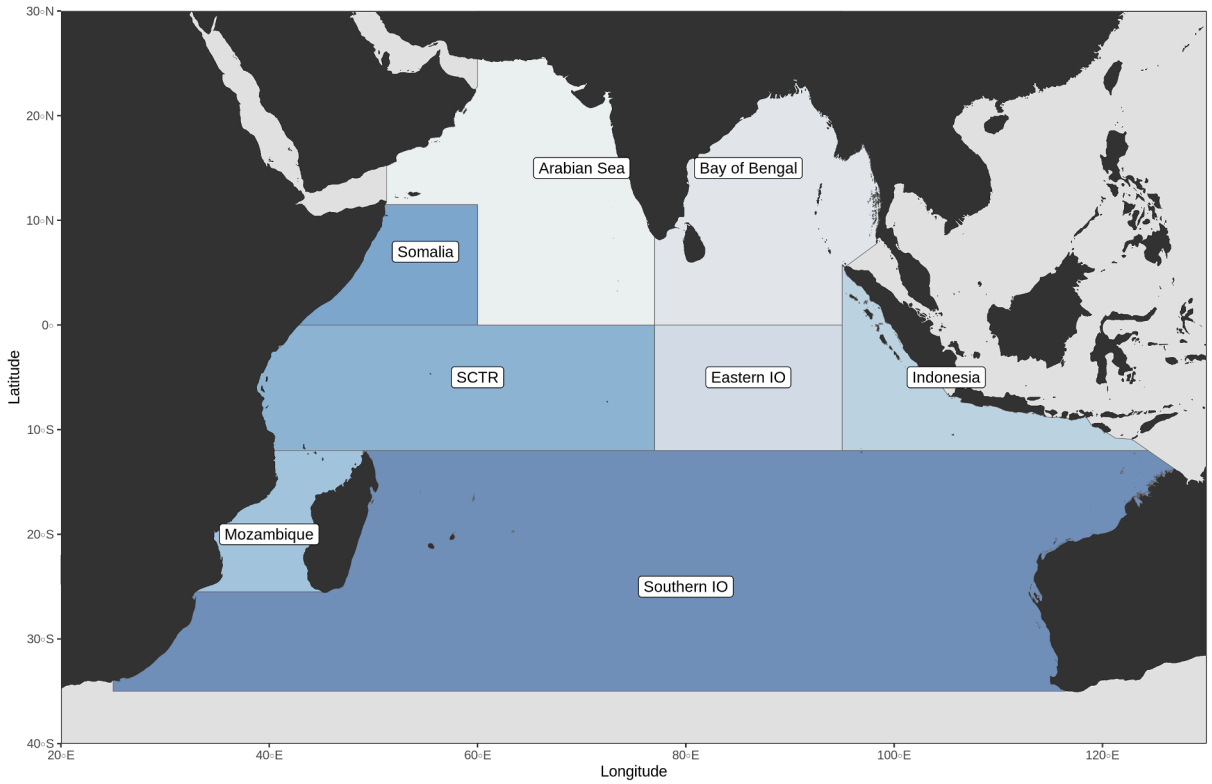


**Fig. 1. Map of the different areas considered in the study**. IO: Indian Ocean. SCTR: Seychelles-Chagos Thermocline Ridge.

days, *i.e.* multiplying by $1-\frac{e^{-\lambda}\lambda^{t}}{t!}$ with $\lambda = 360$ days and $t$ the number of days since release. This approach assumes that NLOGs will sink on average aftre one year, while allowing for some variability in sinking times. The simulations were initiated 500 days before 2000–01-01, to allow the equilibrium to be reached at the beginning of the study period.

### 2.2. Accounting for NLOG release sources and their variability

In order to account for different NLOG sources, as well as potential factors affecting their release rate, we developed different weighting scenarios. For each release location and date, we considered the following factors: (i) associated precipitations, (ii) associated rivers and their discharge and (iii) the surface area covered by forests. Precipitations data at the release location and date were extracted from Adler et al. (2003), which provides global monthly precipitations estimates in mm.days$^{-1}$ per 2° cells. Information about rivers and their discharge were obtained from the HydroAtlas database v1.0 (Linke et al., 2019). Rivers were associated to the nearest release locations considering the position of the river mouth relative to the center of the release cell. We selected rivers with a mouth in the IO and a maximum discharge at the mouth equal to or greater than 100 m$^3$.s$^{-1}$, totaling over 195,000 km of river length in the study region. To account for forest cover, we created a 1 km buffer around the rivers and coastline. We used Global Forest Change products (GFC 2020v1.8, Hansen et al., 2013), which provide time series analysis results of Landsat images, to characterize global forest extent in year 2000 and changes in global forest cover from 2000 to 2020 at 30-meter resolution. The forest cover was mapped in the coastal areas of the IO (Fig. 1) using Google Earth Engine (GEE), an application programming interface (API) using image processing algorithms. The GFC 2020v1.8 product was available in GEE to import GFC global forest extent data in the previously-defined buffer zone for year 2000. For each year after 2000, the GFC pixels (with a resolution of 30 × 30 m$^2$) were successively compared to identify losses and gains of forest area. Yearly raster maps of forest cover were produced, representing forest presence for each pixel with values ranging from 0 (no forest) to 100 % (fully forested pixel). The resolution was then reduced to cells of 90 × 90 m$^2$ size by averaging the pixels.

Six different weighing scenarios were considered, detailed in Table 1 and Fig. 2, allowing to calculate weights associated with each release location-date. For each scenario, the Eulerian fields obtained from the simulations for each release location-date (end of Section 2.1) were multiplied by the associated weight. Estimations of the NLOG

**Table 1**
**Details of the different weighting scenarios.**

| Designation | Details |
|---|---|
| **CL** | **C**oastal **L**ength: in this weighting scenario, particles were uniformly released along the coastline. The weight for each release location-date was determined by measuring the total surface area of the coastline buffer associated to each release location. |
| **CC** | **C**oastal **C**over: this scenario involved releasing particles in proportion to the coastal forest cover. Similar to CL scenario, the weight was calculated based on the coastal forest cover surface associated with each release location and date. |
| **RC** | **R**iver **C**over: in this scenario, particles were released in proportion to the forest cover associated with the rivers and the rivers discharge. For each release location and date, the weight was determined by multiplying the forest cover surface of the associated rivers with the discharge at the rivers' mouths located within each release cell. |
| **CCp** | **C**oastal **C**over and **P**recipitations: this scenario was similar to CC but introduced seasonality by considering precipitations. The weight of each release location and date was calculated by multiplying the corresponding forest cover surface with precipitations. |
| **RCp** | **R**iver **C**over and **P**recipitations: the weighting scenario was similar to RC but introduced seasonality by considering precipitations. The weight was determined by multiplying the forest cover surface of the associated rivers with the discharge at the rivers' mouths and the precipitations at the release location and date. |
| **R&CC** | **R**iver and **C**oastal **C**over: this scenario considered the overall forest cover (both from rivers and coastal areas). For each release location and date, the weight was calculated by summing the coastal forest cover surface and the forest cover surface associated with rivers. |

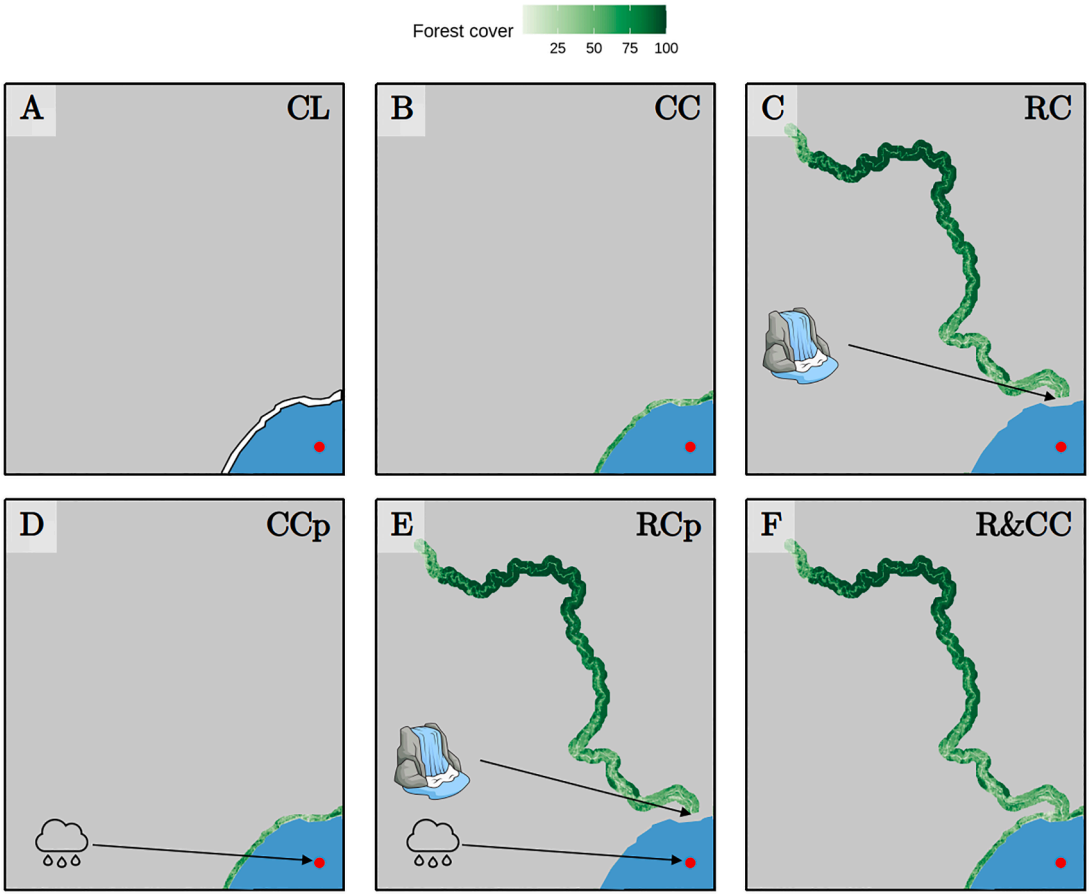


**Fig. 2. Schematic representation of the weighting scenarios used in the study**. The release point is shown in red, forest cover (in % of the cell surface) is represented in green, the land is represented in grey and the sea in blue. (A) CL: total surface of the coastline buffer (white area delineated in black); (B) CC: sum of the forest cover contained in the coastline buffer; (C) RC: sum of the forest cover in the river buffer multiplied by the mean river discharge at river mouth; (D) CCp: CC multiplied by the precipitations at the release point; (E) RCp: RC multiplied by the precipitations at the release point; (F) R&CC: sum of the forest cover in the union of the coastal and river buffers.

abundance were then obtained as follow:

$$N_{i,t} = \sum_{j=1}^{R} \sum_{k=1}^{T} w_{j,t-k} n_{i,t}^{j,t-k} \quad (1)$$

with $N_{i,t}$ the NLOG abundance in cell $i$ at time $t$, $R$ the number of release locations ($R = 6{,}408$), $T$ the duration of a simulation ($T = 500$ days), $w_{j,t-k}$ the weight associated with release location $j$ at time $t-k$ and $n_{i,t}^{j,t-k}$ the number of particles in cell $i$ at time $t$ that were released in release location $j$ at time $t-k$.

### 2.3. Study regions

Simulated NLOG abundances were examined in eight oceanic regions defined on the basis of industrial purse seine fleet behavior in the Western IO (WIO) and oceanographic specificity (Fig. 1; Dagorn et al., 2013a; Schott et al., 2009).

- **Mozambique**: Encompassing the Mozambique Channel, this region is characterized by the presence of numerous oceanic eddies and a dominant southward flowing current throughout the year. Notably, it is known to be rich in NLOGs from March to May, when industrial purse-seine vessels primarily target NLOG-associated tuna schools in this area (Chassot et al., 2019).
- **SCTR** (Seychelles-Chagos Thermocline Ridge): Serving as the central fishing ground of the industrial purse-seine fleets operating in the WIO, this region is marked by a westward current bifurcating northward upon reaching the coast of Madagascar. An open-ocean upwelling structure is present in the area, concentrated in the west from September to February and forming a zonally elongated ridge during the other half of the year (Hermes and Reason, 2008).
- **Somalia**: Known for its strong coastal upwelling during the summer monsoon (July-August) with a northeastward current, this region experiences a reversal of currents during the winter monsoon. It represents an important fishing ground for industrial purse-seine fleets, particularly present in the area after the upwelling, mainly from August to November (Fonteneau, 2003; IOTC, 2022c).
- **Arabian Sea**: This region includes the Arabian Sea and the waters surrounding the Maldives. Surface currents enter the area from the Bay of Bengal during the winter monsoon (January-February) and reverse in the summer monsoon. Industrial purse-seine fishing effort expanded in this region since 2018 (IOTC, 2022c; Tolotti et al., 2022). The region also hosts an important pole-and-line tuna fishery in the Maldivian waters (Jauharee et al., 2021).
- **Bay of Bengal**: this region covers the Bay of Bengal and the area south of Sri Lanka, including the massive Ganges river. It is a relatively enclosed sea, except for a strong entering or exiting current in its western boundary in the summer and winter monsoon respectively.
- **Eastern IO** (Indian Ocean): during the summer monsoon, this region is characterized by a southward current, entering from the Bay of Bengal region and exiting in the Southern IO region, which reverses in the winter monsoon (Schott et al., 2009). During positive Indian

Ocean Dipole (IOD) events, this region is characterized by important negative Sea Surface Temperature (SST) anomalies and a shallower thermocline from July to October (Saji et al., 1999).

- **Indonesia**: This region includes the coastal waters offshore Indonesia, where an important artisanal and semi-industrial tuna fishery operates (IOTC, 2022c). Surface currents flow southward along the coast of Sumatra and are stronger during the winter monsoon. Additionally, a westward current flows in the South of the region, directed towards the Eastern and Southern IO regions (Schott et al., 2009).
- **Southern IO**: Encompassing the entire IO south of 10°S and the region south of Madagascar in the western part of the region, this region is characterized by westward surface currents and minor tropical tuna fishing effort (IOTC, 2022d; Schott et al., 2009).

### 2.4. Comparison with observers data

NLOG positions were derived from data collected by observers on-board French purse seine vessels operating in the WIO from 2014 to 2019. These observer data included the date, time and location of the vessel's main activities. For each activity taking place on a floating object, the object type was recorded, enabling the discrimination of NLOGs from other FOBs like DFADs. Using this dataset, we computed an index of NLOG abundance per 2° cell per month, noted $N^{obs}_{i,m}$ for cell $i$ in month $m$, employing the methodology established in Dupaix et al. (2021a). To account for the data coverage bias stemming from the use of fisheries data, this index is standardized using observation effort. It can be expressed as follows:

$$N^{obs}_{i,m} = \frac{\sum_{d=1}^{D_m} S_{i,d}}{\sum_{d=1}^{D_m} O_{i,d}} \quad (2)$$

where $D_m$ is the number of days in month $m$, $S_{i,d}$ the number of NLOGs observed in cell $i$ on day $d$ and $O_{i,d}$ the number of vessels with an observer in cell $i$ on day $d$. To ensure statistical robustness, cells with a low observation effort ($\sum_{d=1}^{D_m} O_{i,d} < 10$) were discarded. For each of the retained monthly 2° cells, we extracted the corresponding simulated NLOG abundance from the different weighting scenarios. Observed and simulated NLOG abundances were then averaged over the years for each quarter and oceanic region where the French purse seine fleet operates, namely the Arabian Sea, Mozambique, SCTR, Somalia and Southern IO. For each scenario, a linear regression was performed between the observed and simulated NLOG abundances to determine which scenario performed the best and a Student's t-test was performed to determine if the slope coefficient of the linear regression significantly differed from zero.

### 2.5. Assessing NLOG density in the IO

Using the outcome of the different scenarios described in Section 2.2, we calculated NLOG densities on a weekly basis, by averaging the estimated NLOG abundances per unit surface over each oceanic region. To standardize density estimations, these values were divided by the NLOG density averaged over the whole study period in each region. Next, we used these standardized weekly density estimates to calculate the mean weekly values over the whole study period for each region and for the entire oceanic basin, giving access to seasonal variations.

We calculated a weekly NLOG density anomaly (noted $A_t$, where $t$ is the time) by removing the seasonal variations from the standardized weekly density estimations. To assess the presence or absence of any global increasing or decreasing trend in NLOG density across the oceanic basin, linear regressions were performed on $A_t$, with time as an explanatory variable ($A_t = at + b$). To evaluate temporal autocorrelation, we calculated the Pearson's correlation coefficient ($\rho$) between $A_t$ and $A_{t-\Delta t}, \forall \Delta t \in \{0, 1, \ldots, 52\}$, with $\Delta t$ in weeks. We then determined the maximum time lag ($\Delta t_m$) for which $\rho \geqslant 0.2$, *i.e.* $\Delta t_m = \max(\Delta t / \rho(A_t, A_{t-\Delta t}) \geqslant 0.2)$. A Student t-test was then performed to evaluate if the slope coefficient ($a$) significantly differed from zero. The test uses $\frac{\sqrt{s-2}}{\sqrt{\Delta t_m}}$ degrees of freedom, with $s$ representing the number of values in the time series.

## 3. Results

### 3.1. Best performing scenarios

Fig. 3 displays the comparison between observed and simulated NLOG abundances within the oceanic regions and quarters sampled by scientific observers on-board purse seiners (see Section 2.4). The Coastline Length (CL) scenario notably overestimates NLOG density in the Arabian Sea and Somalia in the 3rd quarter, and underestimates the NLOG abundance in the Mozambique Channel, resulting in a non-significant relationship between modelled and observed NLOG abundances between regions and seasons (p-value $= 0.97$). Simulated NLOG abundances obtained with other scenarios display a significant linear relationship with the observed NLOG abundance (linear regressions, p-value of $1.67 \times 10^{-4}, 9.98 \times 10^{-5}, 4.06 \times 10^{-4}, 1.36 \times 10^{-4}$ and $1.61 \times 10^{-4}$ for CC, RC, CCp, RCp and R&CC scenarios respectively).

In summary, CL is the scenario performing the worst, highlighting the need to take forest cover into account. However, this comparison with data does not allow to determine a scenario that would perform better than others, with $R^2$ values ranging from 0.73 to 0.79. Most scenarios tend to overestimate NLOG abundance in some regions at given quarters (*e.g.* Arabian Sea and Somalia regions in the third quarter), and the significant linear relationships are mostly driven by the values observed and simulated in the Mozambique Channel.

### 3.2. Distribution of NLOGs in the Indian Ocean

Fig. 4 displays simulated climatological NLOG density maps for the different scenarios. Among all scenarios, the Mozambique Channel, the Bay of Bengal and the western coast of India exhibited the highest NLOG densities, designating them as probable sources (*i.e.* regions with an important input) and accumulation zones of NLOGs in the IO. However, the relative importance of these areas strongly varies as a function of the scenario considered. In the CL scenario (Coastal Length, uniform release along the coast), the highest densities are located along the coast of India and in the Bay of Bengal, with relatively lower densities in the Mozambique Channel (Fig. 4A). Considering the coastal cover (scenarios CC and CCp) increased the relative density in the Mozambique Channel and more broadly across the rest of the oceanic basin, specifically in Somalia, Eastern IO and Southern IO regions (Fig. 4B&D). Increased NLOG densities in the Southern IO region for scenarios CC and CCp can be explained through an increased relative NLOG density on the coast of Sumatra (Indonesia region) which suggests that the coastal forest cover in this area could also constitute a potential source of NLOGs. In scenarios incorporating river cover (RC and RCp), the NLOG density in the Bay of Bengal was notably higher than in any other region, with a very high density in the south of Myanmar, likely originating from the Ganges delta (Fig. 4C&E). The R&CC scenario (Fig. 4F) displayed intermediate NLOG distribution, falling between those obtained with coastal cover only (CC and CCp) and with river cover only (RC and RCp). In summary, all scenarios designate the Mozambique Channel, the Bay of Bengal, the western coasts of India and Sumatra as the main sources of NLOGs, which then drift towards the oceanic basin. NLOGs originating from the Mozambique Channel feed the WIO (West of SCTR, Somalia and South of Arabian Sea regions), while the Bay of Bengal and the western coasts of India and Sumatra, feed the Eastern and Southern IO regions.

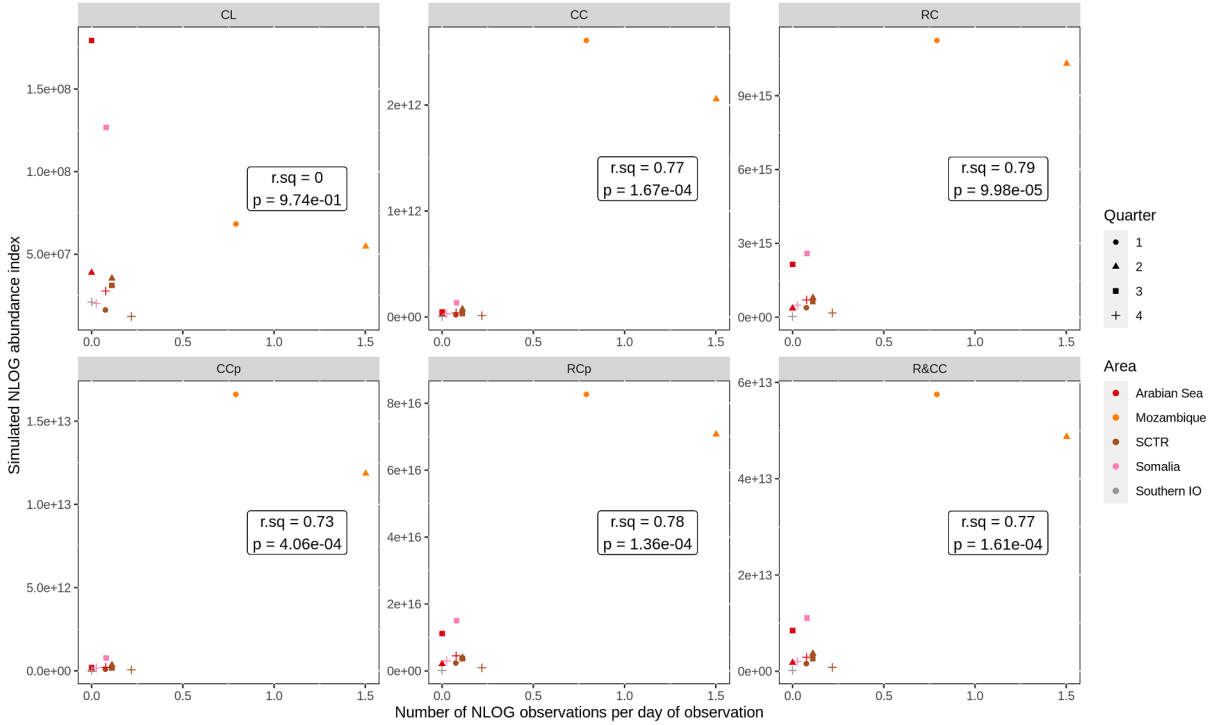


**Fig. 3. Comparison between simulated and observed NLOG abundance for each weighting scenario.** y-axis: NLOG abundance index obtained from simulations, corresponding to the number of simulated NLOGs per 2° cell. x-axis: NLOG abundance index obtained from observers data, corresponding to the number of observed NLOGs per day of observation. CL: Coastline Length; CC: Coastal forest Cover; RC: River forest Cover multiplied by river discharge; CCp: Coastal forest Cover multiplied by precipitations; RCp: River forest Cover multiplied by river discharge and by precipitations; R&CC: River plus Coastal forest Cover. SCRT: Seychelles-Chagos Thermocline Ridge. On each panel, r.sq: $R^2$ of the linear regression; p: p-value of the Student's t-test testing if the slope coefficient of the linear relationship significantly differs from zero. Because values from observers data and from simulations correspond to different indices of NLOG abundance, this figure does not allow for quantitative comparisons.

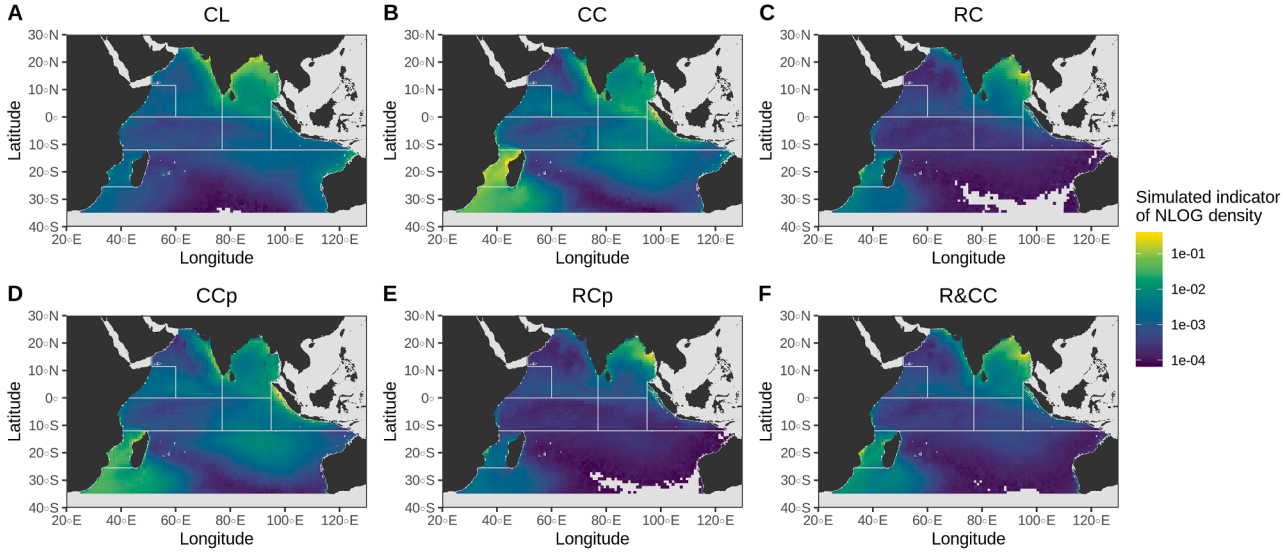


**Fig. 4. Simulated density of NLOGs averaged over 2000–2019 for the different weighting scenarios.** Maximum value was set to 1 and values below $10^{-4}$ were discarded. CL: Coastline Length; CC: Coastal forest Cover; RC: River forest Cover multiplied by river discharge; CCp: Coastal forest Cover multiplied by precipitations; RCp: River forest Cover multiplied by river discharge and by precipitations; R&CC: River plus Coastal forest Cover.

### 3.3. Seasonal variations of NLOG density

Fig. 5 illustrates the seasonal variations in NLOG densities. In some regions (Arabian Sea, Eastern IO, SCTR and Somalia), these variations were marginally influenced by the type of scenario, indicating that the seasonality was mainly driven by the seasonality of the surface currents rather than by that of NLOG inputs. Density maxima were observed in the Arabian Sea between February and May, in the Eastern IO between August and November, in the SCTR between March and April and in Somalia in August (Fig. 5A,C,F&G). However, small differences between

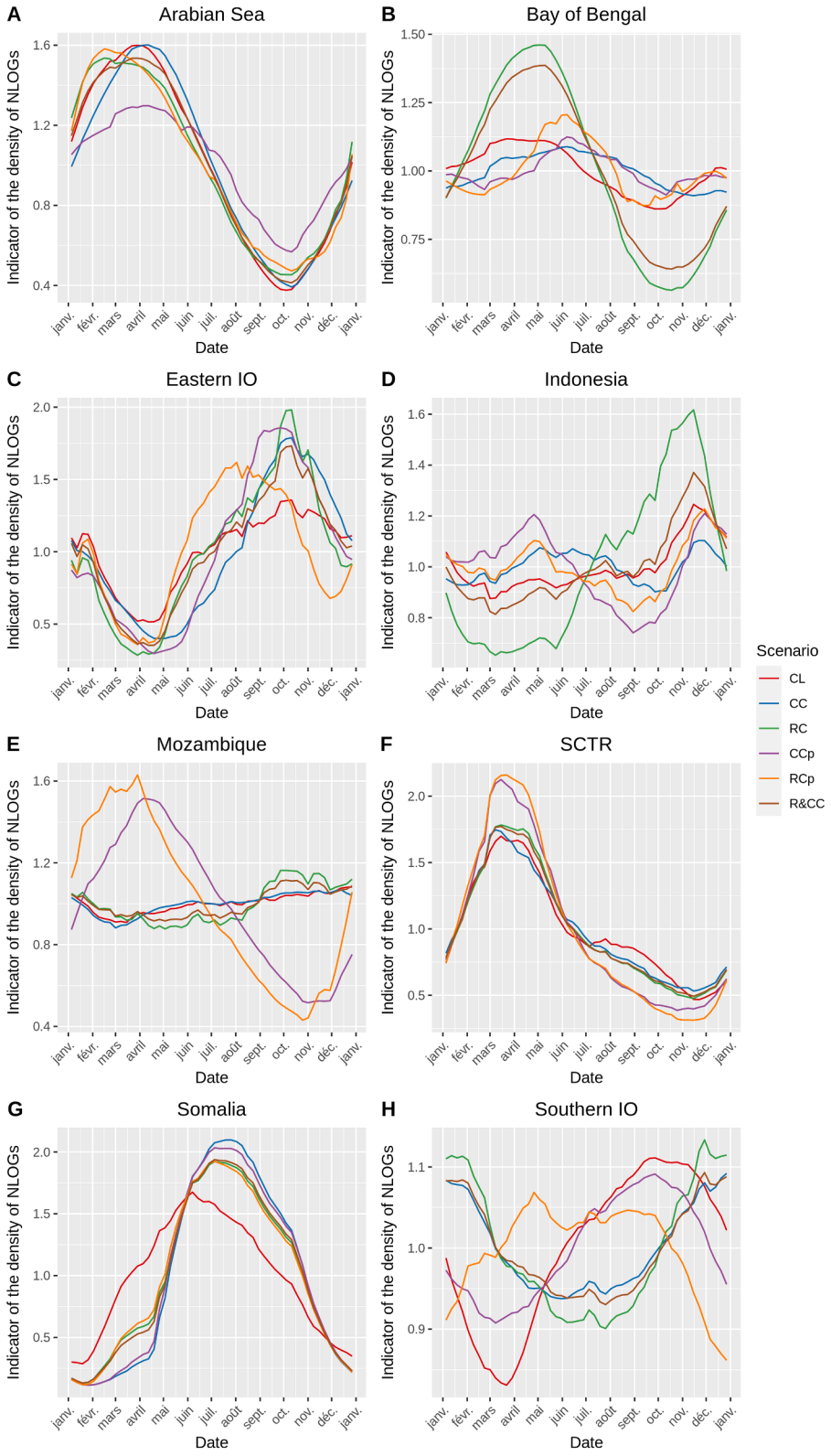


**Fig. 5. Average variations of mean simulated density of NLOGs per area.** The densities are scaled for each scenario and area. Note that the scales do not allow for direct comparison between different areas. CL: Coastline Length; CC: Coastal forest Cover; RC: River forest Cover multiplied by river discharge; CCp: Coastal forest Cover multiplied by precipitations; RCp: River forest Cover multiplied by river discharge and by precipitations; R&CC: River plus Coastal forest Cover. IO: Indian Ocean; SCTR: Seychelles-Chagos Thermocline Ridge.

scenarios were still noticeable. For example, in the Eastern IO, the density maximum occurred from July to November depending on the scenario (Fig. 5C). Similarly, in Somalia, the CL scenario showed an earlier maximum compared to other scenarios (Fig. 5G). On the other hand, in the Bay of Bengal, Indonesia, Mozambique and Southern IO, the seasonality varied depending on the considered scenario (Fig. 5B,D, E&H). In the Bay of Bengal, scenarios considering the river forest cover displayed a strong seasonality, with a density peak in May (RC and R&CC), while accounting for precipitations partially compensated for this seasonality and resulted in a smaller density peak later in June-July (CCp and RCp, Fig. 5B). Noticeably, in the Bay of Bengal, the Ganges river constitutes by far the main source of NLOGs. The strong seasonality observed in scenarios RC and R&CC could be due to the reverse of currents in the area, which provokes the retention around May and the stranding and/or exit of particles originating from the Ganges in other periods of the year. In the Indonesia region, scenarios accounting for precipitations (CCp and RCp) predicted a maximum density in the first half of the year, which is in agreement with the higher precipitations observed in the area from November to April (Figure S1 in Supplementary Materials). However, considering rivers led a maximum density being observed in the second half of the year in the Indonesia region (RC and R&CC, Fig. 5D). In the Mozambique region, very few seasonal variations were observed except in scenarios considering the precipitations, where the maximum density occurred in February-April and in April-May for the CCp and RCp scenarios, respectively (Fig. 5E).

### 3.4. Trends of NLOG numbers in the Indian Ocean

Fig. 6 depicts the variations in simulated NLOG density anomalies, estimated over the entire oceanic basin, from 2000 to 2019. Among all scenarios, only the CL scenario exhibited a significant positive trend (p. value $4.4 \times 10^{-2}$, Table 2). For CC and CCp scenarios, there was a non-significant increasing trend (p.values $6.3 \times 10^{-2}$ and $2.8 \times 10^{-1}$ respectively). However, when considering the river forest cover (RC, RCp and R&CC), the mean NLOG density showed a non-significant decreasing trend (p.values $6.6 \times 10^{-1}$, $8.8 \times 10^{-1}$ and $5.2 \times 10^{-1}$ respectively). In the CL scenario, where the total weight applied to released particles remained constant over the years (Figure S2 in Supplementary Materials), the slightly positive trend must originate from changes in currents that could lead to higher particles retention within the oceanic basin. Including a decreasing coastal forest cover over the years did not compensate for this trend due to surface current changes, resulting in the positive but non-significant trends observed in the CC and CCp scenarios. However, when considering the forest cover associated with river basins (RC, RCp), the previously observed increasing trend was reversed, although it remained non-significant. This reversal might be attributed to loss of forest cover over the study period, but also to changes in surface currents as the decrease of the total number of weighted particles released was greater for the CC scenario than for the

**Table 2**
**Results of the linear regressions performed between the NLOG density anomaly ($A$) and time**, represented on Fig. 6, for the different weighting scenarios. Significant slope coefficients are in bold. $\Delta t$: maximum time lag such that Pearson's correlation coefficient $\rho(A_t, A_{t-\Delta t}) \geqslant 0.2$. CL: Coastline Length; CC: Coastal forest Cover; RC: River forest Cover multiplied by river discharge; CCp: Coastal forest Cover multiplied by precipitations; RCp: River forest Cover multiplied by river discharge and by precipitations; R&CC: River plus Coastal forest Cover.

| Scenario | Slope estimate (% per day) | $\Delta t$ (weeks) | p-value |
|---|---|---|---|
| CL | $\mathbf{3.4 \times 10^{-5}}$ | 21 | $4.4 \times 10^{-2}$ |
| CC | $8.4 \times 10^{-5}$ | 29 | $6.2 \times 10^{-1}$ |
| RC | $-8.2 \times 10^{-6}$ | 25 | $6.6 \times 10^{-1}$ |
| CCp | $3.0 \times 10^{-5}$ | 29 | $2.8 \times 10^{-1}$ |
| RCp | $-6.1 \times 10^{-5}$ | 31 | $8.8 \times 10^{-1}$ |
| R&CC | $-1.0 \times 10^{-6}$ | 30 | $5.2 \times 10^{-1}$ |

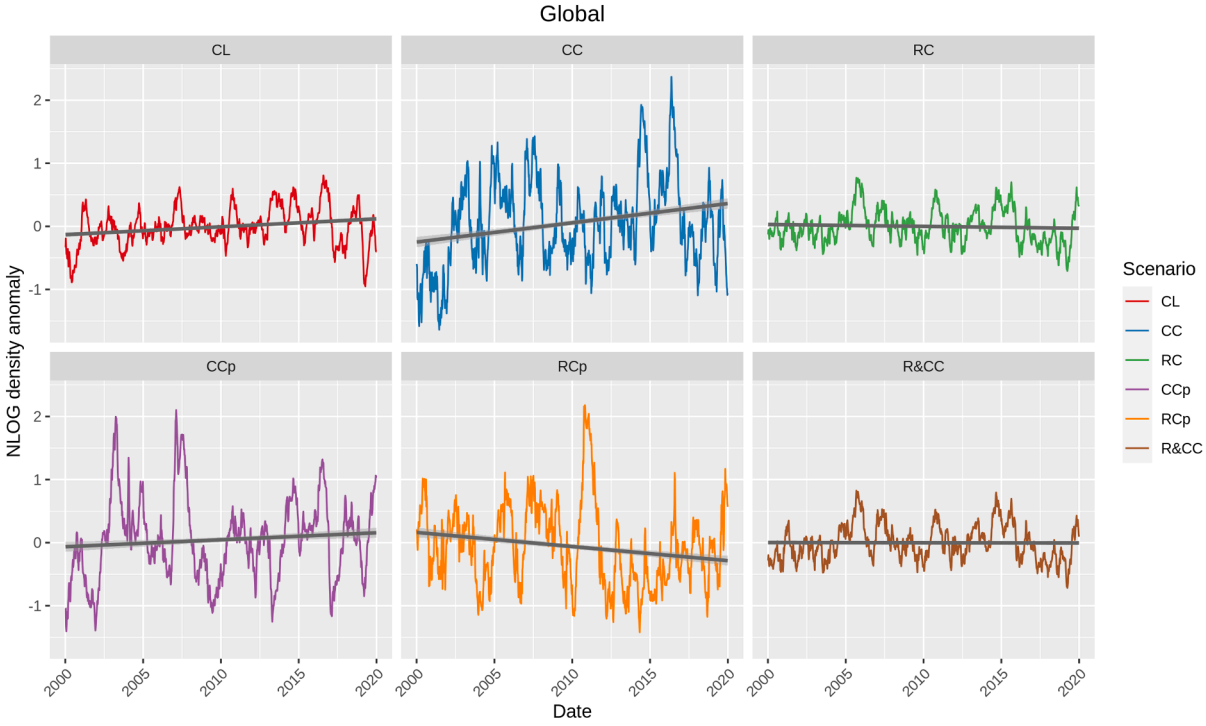


**Fig. 6. Anomaly of the simulated density of NLOGs from 2000 to 2019, averaged over the entire Indian Ocean**. The NLOG density anomaly was obtained by substracting mean seasonal variations from the raw densities. The grey line represents a linear regression between the NLOG density anomaly and time. CL: Coastline Length (corrected p.value for linear regression slope significance: $4.4 \times 10^{-2}$); CC: Coastal forest Cover (corrected p.value $6.2 \times 10^{-1}$); RC: River forest Cover multiplied by river discharge (corrected p.value $6.6 \times 10^{-1}$); CCp: Coastal forest Cover multiplied by precipitations (corrected p.value $2.8 \times 10^{-1}$); RCp: River forest Cover multiplied by river discharge and by precipitations (corrected p.value $8.8 \times 10^{-1}$); R&CC: River plus Coastal forest Cover (corrected p.value $5.2 \times 10^{-1}$).

RC scenario (Figure S2 in Supplementary Materials).

## 4. Discussion

This study provides the first-ever estimations of relative densities of natural floating objects (NLOG) at the scale of the Indian Ocean, offering insights into their seasonal and long-term variability. These estimations are an important step towards better understanding the impact of human activities on this important component of marine habitats. All tested scenarios indicate that the areas with highest NLOG densities are the Bay of Bengal, the Mozambique Channel and the Eastern Arabian Sea. Considering either the coastal forest cover or the forest cover associated with rivers did not induce any change in the goodness-of-fit of the different scenarios, when comparing the predicted NLOG abundances with those derived from observers data in the WIO. All scenarios suggest no decreasing trend in NLOG densities across the entire IO, despite the observed loss of forested lands globally (Figure S2 in Supplementary Materials, IPBES, 2019). Instead, our results suggest that the loss of coastal forest was compensated by a change in surface currents. This change resulted in a higher proportion of NLOGs being retained in the IO, whereas they would have drifted to adjacent oceans earlier in the study period. Most areas did not display any significant trend over the study period, except for the Arabian Sea in the CL and CC scenarios (corrected p.values $3.7 \times 10^{-2}$ and $1.2 \times 10^{-2}$ respectively; Figures S3&S4 and Table S1 in Supplementary Materials). However, although non-significant, the slope coefficients in some areas were negative whatever the scenario (*e.g.* Eastern IO, Somalia and Indonesia), suggesting that potential decreasing trends in these areas might be observed over longer study periods. Overall, these findings highlight the complex and region-specific dynamics influencing NLOG densities in the Indian Ocean.

Van der Stocken et al. (2019) conducted simulations on the global dispersion of mangrove propagules and found high densities in the Mozambique Channel, Bay of Bengal and in the Eastern Arabian Sea. The global density patterns obtained in our study also align with Lagrangian simulations performed to determine the global distribution of plastics debris or microplastics (Van Sebille et al., 2015; Viatte et al., 2020). However, these studies on plastic distribution identified an accumulation area in the eastern southern IO, which was not present in our simulations. This discrepancy could be attributed to difference in drift time used in the simulations. In Van Sebille et al. (2018) and Viatte et al. (2020), simulations were carried out with much longer drift times, ranging from 20 to 50 years, emphasizing the importance of carefully considering particles lifetimes (Crochelet et al., 2020; Stelfox et al., 2020). Considering that estimations of driftwood lifetimes range from a few days to 1000 days (Thiel and Gutow, 2005) and previous simulations showed little effect of drift time on our simulations (Dupaix et al., 2021a), we are confident that simulating NLOG drift for 360 days was appropriate. Confirmation of these simulated drift times could be achieved by conducting field-based estimations of NLOG drifting times through the study of fixed organisms and wood degradation. However, such estimations are challenging due to the dependence of wood colonization by fixed organisms on the richness of the crossed zones, and the variability of wood degradation based on species characteristics (Russell et al., 2014). Additionally, limited information exists on the tree species found at sea, further complicating such estimates. Alternative methodologies to determine drift times could involve the use of backward-in-time lagrangian simulations using NLOGs observed at sea as release locations. Furthermore, the duration for which echosounder buoys, deployed on both DFADs and NLOGs by purse seine fleets, remain active, could also provide insight into the drifting time of NLOGs. However, echosounder buoys are deployed on NLOGs which are already at sea and can be deactivated remotely, making them suitable only as a lower bound for drift time estimates.

When comparing the results obtained through the simulations with observers data, most scenarios apart from the CL performed well. However, the goodness-of-fit of estimated NLOG abundances was strongly driven by high NLOG abundance indices recorded in the Mozambique Channel (Fig. 3). Improved validation of the best performing scenarios could be obtained by including more field data, specifically from areas and/or time periods beyond those present in the observers data used in this study. The inspection of seasonal patterns (Fig. 5) allowed to highlight further specific features related to each weighting scenario. Industrial purse seine fleets in the IO primarily fish in the Mozambique Channel from March to May (IOTC, 2022d), mainly targeting tuna associated with natural floating objects since the early days of the fishery (Fonteneau, 2003; IOTC, 2022d). This seasonal behavior of the fleet may indicate that scenarios CCp and RCp can best reproduce the expected seasonal patterns of NLOG density in this area, highlighting the need to take precipitations into account. However, it remains unclear whether the absence of NLOGs in the Mozambique area during the rest of year explains the lack of purse seine fishing activity or if other oceanographic factors, such as the upwelling in the Somalia area during the summer monsoon (July-August; Schott et al., 2009), redirect fishers to different areas. In the Maldives, pole-and-line fishers target NLOG-associated tuna from December to April and in October Jauharee et al. (2021). Our findings with all scenarios are consistent with this seasonal patterns in the Maldivian fishery during the first part of the year (Dec-Apr, Fig. 5A). However, no scenario suggest any increase of NLOG density in the Arabian Sea in October. It is essential to note that the Arabian Sea area used in this study is much larger than the waters surrounding the Maldives. When examining quarterly simulated density maps, the scenario that aligns best with Jauharee et al. (2021)'s results would be the RCp scenario (Figure S5 in Supplementary Materials). The simulations presented here can be complemented by more localized studies in areas where fishers use NLOGs, relying on Local Ecological Knowledge to improve the proposed scenarios.

The significant modifications of pelagic surface habitat caused by DFADs have led scientists to hypothesize that DFADs could indirectly impact tropical tunas and act as an "ecological trap" (Marsac et al., 2000; Hallier and Gaertner, 2008). An ecological trap occurs when individuals select habitat that no longer offer suitable conditions due to anthropic changes, negatively affecting their fitness and potentially impacting the population (Battin, 2004; Gilroy and Sutherland, 2007; Swearer et al., 2021). The *indicator-log* hypothesis suggests that tuna would associate with NLOGs to find biologically productive areas, as NLOGs originate from rivers and accumulate in rich frontal zones (Fréon and Dagorn, 2000; Castro et al., 2002). The ecological trap hypothesis applied to DFADs and tropical tuna proposes that DFADs could alter the density and distribution of FOBs, potentially leading to the retention or transport of tuna to poorly productive or unsuitable areas Marsac et al. (2000). If NLOGs densities decrease in historically high-density areas, and if these areas are still productive, it could exacerbate this ecological trap. However, the scenarios developed in this study (CC, RC, CCp, RCp and R&CC) predicted no significant trends of NLOG numbers in the Bay of Bengal and in the Mozambique Channel, the areas with highest simulated NLOG densities.

The increase in FOB density induced by DFADs may have other potential indirect ecological impacts on tuna. It could lead to increased time spent by tuna associated with FOBs and disturb their schooling behavior (Fréon and Dagorn, 2000; Pérez et al., 2020; Soria et al., 2009). The *meeting-point* hypothesis is another hypothesis explaining the associative behavior of tuna, positing that tuna use FOBs to facilitate encounters with conspecifics and promote schooling behaviour (Fréon and Dagorn, 2000). An increase of FOB density could disperse tuna among FOBs and hinder the formation of large schools (Capello et al., 2022; Sempo et al., 2013). An increase in NLOG density despite forest cover loss (as suggested by the CC and CCp scenarios) could potentially compound the impacts of DFADs on schooling behavior.

FOBs play a crucial role in marine species' habitat, benefiting a wide range of species from fixed organisms to large pelagic predators (Fréon and Dagorn, 2000; Thiel and Gutow, 2005). In recent decades, human

activities, such as fishing, plastic waste, logging and agriculture, have significantly altered their distribution (Dupaix et al., 2021a; Thiel and Gutow, 2005; Van Sebille et al., 2015). While large plastic debris distribution is well-studied (Mendenhall, 2018), the impacts of DFAD fishing and other human activities on FOB distribution remain relatively unknown. Studies have mainly focused on the WIO and Western and Central Pacific Ocean, considering NLOGs as a reference, and have shown that DFADs strongly increase the number of FOBs at sea (Dagorn et al., 2013a; Dupaix et al., 2021a; Phillips et al., 2019). However, the impact of other human activities like agriculture or logging (causing deforestation) has not been extensively studied. This study, showing limited influence of human activities on NLOG numbers but strong seasonal variations, is an initial step towards better understanding this important component of marine habitats.

This study aims to establish a baseline understanding of the respective contribution of currents variations and deforestation on the distribution of floating objects in the Indian Ocean, focusing on a well-sampled period (2000–2019). However, the relatively short time frame considered in this study does not allow for a clear separation between the influences of climate change and natural climate variability on surface currents trends. The methodology presented here could be adapted to partly address the impact of human-induced climate change on the future distribution of NLOGs. This adaptation would involve using future flow fields from Earth System Models (ESMs) rather than current conditions. However, several challenges complicate this approach, including the lack of reliable future deforestation projections (Teo et al., 2023) and the coarse horizontal resolution of ESMs, which often fail to adequately capture meso-scale eddies. Moreover, ESMs exhibit significant biases in their representation of present-day currents, which could undermine the reliability of any conclusions drawn about future scenarios (Hewitt et al., 2020; Zhang and Wang, 2023). Despite these limitations, evaluating the impact of future flow evolution on NLOG distribution could still be possible at a coarser resolution than what was achieved in this study, and under the assumption that deforestation rates remain similar with current observations. However, such an analysis remains beyond the scope of our current work and is left for future studies.

This study presents first-ever simulations assessing the long-term impacts of terrestrial human activities on a crucial natural component of the pelagic surface habitat. Our results not only provide estimates of NLOG density across the entire IO but also enable more accurate local estimations of NLOG densities and variations than previous studies based on fisheries data (Dupaix et al., 2021a). These local estimates, which can still be further refined, can be invaluable for fisheries management and ecological studies aiming to understand the effects of DFAD fisheries on tropical tuna and other species associating with FOBs. The simulations reveal diverse trends across regions, although many are not statistically significant (see Figures S3&S4 in Supplementary Materials), warranting further exploration through Local Ecological Knowledge in areas where fisheries rely on driftwood to enhance their tuna catches (Western Indian Ocean, Indonesia, Maldives; Moreno et al., 2007; Jauharee et al., 2021). The different scenarios, based on coastal forest cover and/or river associated forest cover, suggest no significant increase in average NLOG densities in the ocean. However, these findings underscore the limited understanding of this critical element of pelagic species habitat and the need to assess habitat modifications on an even longer term to determine climate change impacts. Therefore, there is pressing need to intensify monitoring efforts for pelagic species habitat and raise awareness about potential indirect impacts of habitat modifications on tuna and other pelagic species (Dupaix et al., 2024). These impacts should be further investigated and better considered by regional fisheries management organizations to ensure the sustainable management of marine resources.

## Declaration of Competing Interest

The authors declare that they have no known competing financial interests or personal relationships that could have appeared to influence the work reported in this paper.

## Data availability

Data will be made available on request.

## Acknowledgements

This work was supported by the TREES@SEA project (Labex CEMEB; URL: https://umr-marbec.fr/en/the-projects/trees_sea/). Observer data have been collected through the Data Collection Framework (Reg 2017/1004 and 2016/1251) funded both by IRD and the European Union since 2005, and OCUP ("Observateur Commun Unique et Permanent"), an industry-funded program coordinated by ORTHONGEL since 2014. We sincerely thank IRD's Ob7 ("Observatoire des Ecosystèmes Pélagiques Tropicaux Exploités") in charge of observer data collection, processing, management, and for sharing the data used in this study. We also acknowledge the Pôle de Calcul et des Données Marines (PCDM) for providing DATARMOR storage, data access, computational resources, visualization, web-services, consultation and support services (URL: https://pcdm.ifremer.fr/). We also acknowledge the anonymous reviewers for their extensive and constructive feedback.

## Appendix A. Supplementary material

Supplementary data associated with this article can be found, in the online version, at https://doi.org/10.1016/j.gloenvcha.2024.102917.

## References

Adler, R.F., Huffman, G.J., Chang, A., Ferraro, R., Xie, P.-P., Janowiak, J., Rudolf, B., Schneider, U., Curtis, S., Bolvin, D., Gruber, A., Susskind, J., Arkin, P., Nelkin, E., 2003 The Version 2 Global Precipitation Climatology Project (GPCP) Monthly Precipitation Analysis (1979–Present). Journal of Hydrometeorology, 4, 1147–1167. URL: https://journals.ametsoc.org/view/journals/hydr/4/6/1525-7541_2003_004_1147_tvgpcp_2_0_co_2.xml. Publisher: American Meteorological Society Section: Journal of Hydrometeorology.

Andrello, M., Guilhaumon, F., Albouy, C., Parravicini, V., Scholtens, J., Verley, P., Barange, M., Sumaila, U.R., Manel, S., Mouillot, D., 2017. Global mismatch between fishing dependency and larval supply from marine reserves. Nature Communications, 8, 16039. URL: https://www.nature.com/articles/ncomms16039. Number: 1 Publisher: Nature Publishing Group.

Barrier, N., Verley, P., Andres, G., Lett, C., 2023 Ichthyop: A Lagrangian tool for modelling ichthyoplankton dynamics. URL: doi: 10.5281/zenodo.6520064.

Battin, J., 2004 When Good Animals Love Bad Habitats: Ecological Traps and the Conservation of Animal Populations. Conservation Biology, 18, 1482–1491. URL: https://conbio.onlinelibrary.wiley.com/doi/abs/10.1111/j.1523-1739.2004.00417.x. L.

Bessières, L., Leroux, S., Brankart, J.-M., Molines, J.-M., Moine, M.-P., Bouttier, P.-A., Penduff, T., Terray, L., Barnier, B., Sérazin, G., 2017. Development of a probabilistic ocean modelling system based on NEMO 3.5: Application at eddying resolution. Geoscientific Model Development, 10, 1091–1106. Publisher: Copernicus GmbH.

Caddy, J.F., Majkowski, J., 1996. Tuna and trees: a reflection on a long-term perspective for tuna fishing around floating logs. Fisheries Research, 25, 369–376. URL: http://www.sciencedirect.com/science/article/pii/0165783695004491.L.

Capello, M., Merino, G., Tolotti, M., Murua, H., Dagorn, L., 2023 Developing a science-based framework for the management of drifting Fish Aggregating Devices. Marine Policy, 153, 105657. URL: https://www.sciencedirect.com/science/article/pii/S0308597X23001847.L.

Capello, M., Rault, J., Deneubourg, J.-L., Dagorn, L., 2022. Schooling in habitats with aggregative sites: The case of tropical tuna and floating objects. J. Theor. Biol. 547, 111163. URL: https://www.sciencedirect.com/science/article/pii/S0022519322001618.

Castro, J.J., Santiago, J.A. and Santana-Ortega, A.T., 2002. A general theory on fish aggregation to floating objects: An alternative to the meeting point hypothesis. Reviews in Fish Biology and Fisheries, 11, 255–277. L.

Chassot, E., Bodin, N., Sardenne, F., Obura, D., 2019. The key role of the Northern Mozambique Channel for Indian Ocean tropical tuna fisheries. Rev. Fish Biol. Fisheries 29, 613–638. https://doi.org/10.1007/s11160-019-09569-9.

Crochelet, E., Barrier, N., Andrello, M., Marsac, F., Spadone, A., Lett, C., 2020. Connectivity between seamounts and coastal ecosystems in the Southwestern Indian

Ocean. Deep Sea Res. Part II 176, 104774. URL: https://linkinghub.elsevier.com/retrieve/pii/S0967064519301080.
Curnick, D.J., Feary, D.A., Cavalcante, G.H., 2021. Risks to large marine protected areas posed by drifting fish aggregation devices. Conservation Biology, 35, 1222–1232. URL: https://conbio.onlinelibrary.wiley.com/doi/abs/10.1111/cobi.13684.L.
Dagorn, L., Bez, N., Fauvel, T., Walker, E., 2013a. How much do fish aggregating devices (FADs) modify the floating object environment in the ocean? Fisheries Oceanography, 22, 147–153. URL: http://doi.wiley.com/10.1111/fog.12014. L.
Dagorn, L., Holland, K.N., Restrepo, V., Moreno, G., 2013b. Is it good or bad to fish with FADs? What are the real impacts of the use of drifting FADs on pelagic marine ecosystems? Fish Fish. 14, 391–415. URL: http://doi.wiley.com/10.1111/j.1467-2979.2012.00478.x. L.
Davies, T., Curnick, D., Barde, J., Chassot, E., 2017. Potential environmental impacts caused by beaching of drifting fish aggregating devices and identification of management solutions and uncertainties. Ad-hoc Working Group on FADs IOTC-2017-WGFAD01-08, Indian Ocean Tuna Commission. L.
Davies, T.K., Mees, C.C., Milner-Gulland, E., 2014 The past, present and future use of drifting fish aggregating devices (FADs) in the Indian Ocean. Marine Policy, 45, 163–170. URL: https://linkinghub.elsevier.com/retrieve/pii/S0308597X13002972. L.
Doong, D.-J., Chuang, H.-C., Shieh, C.-L., Hu, J.-H., 2011. Quantity, distribution, and impacts of coastal driftwood triggered by a typhoon. Marine pollution bulletin, 62, 1446–1454. L.
Dupaix, A., Capello, M., Lett, C., Andrello, M., Barrier, N., Viennois, G., Dagorn, L., 2021a. Surface habitat modification through industrial tuna fishery practices. ICES J. Mar. Sci. 78, 3075–3088.
Dupaix, A., Ménard, F., Filmalter, J.D., Baidai, Y., Bodin, N., Capello, M., Chassot, E., Demarcq, H., Deneubourg, J.-L., Fonteneau, A., Forget, F., Forrestal, F., Gaertner, D., Hall, M., Holland, K.N., Itano, D., Kaplan, D.M., Lopez, J., Marsac, F., Maufroy, A., Moreno, G., Muir, J.A., Murua, H., Roa-Pascuali, L., Pérez, G., Restrepo, V., Robert, M., Schaefer, K.M., Sempo, G., Soria, M., Dagorn, L., 2024. The challenge of assessing the effects of drifting fish aggregating devices on the behaviour and biology of tropical tuna. Fish Fish. 25, 381–400.
Dupaix, A., Mérillet, L., Kopp, D., Mouchet, M., Robert, M., 2021b. Using biological traits to get insights into the bentho-demersal community sensitivity to trawling in the Celtic Sea. ICES J. Mar. Sci. 78, 1063–1073.
Dussin, R., Barnier, B., Brodeau, L., Molines, J.M., 2016. Drakkar forcing set DFS5. Tech. rep., MyOcean Report.
Fonteneau, A., 2003. Prospects for the management of FAD fisheries in the Indian Ocean. IOTC Proc. 6, 030–047.
Fonteneau, A., Chassot, E., Bodin, N., 2013. Global spatio-temporal patterns in tropical tuna purse seine fisheries on drifting fish aggregating devices (DFADs): Taking a historical perspective to inform current challenges. Aquatic Living Resources, 26, 37–48. L.
Fontoura, L., D'Agata, S., Gamoyo, M., Barneche, D.R., Luiz, O.J., Madin, E.M.P., Eggertsen, L., Maina, J.M., 2022. Protecting connectivity promotes successful biodiversity and fisheries conservation. Science, 375, 336–340. URL: https://www.science.org/doi/10.1126/science.abg4351. Publisher: American Association for the Advancement of Science.
Fréon, P., Dagorn, L., 2000. Review of fish associative behaviour: toward a generalisation of the meeting point hypothesis. Reviews in Fish Biology and Fisheries, 10, 183–207. L.
Gershman, D., Nickson, A., O'Toole, M., 2015. Estimating the Use of FADs Around the World. Tech. rep., PEW Charitable Trusts. URL: http://pew.org/1XUPV4w.L.
Gilroy, J., Sutherland, W., 2007. Beyond ecological traps: perceptual errors and undervalued resources. Trends in Ecology & Evolution, 22, 351–356. URL: https://linkinghub.elsevier.com/retrieve/pii/S016953470700105X.L.
Hallier, J.-P., Gaertner, D., 2008. Drifting fish aggregation devices could act as an ecological trap for tropical tuna species. Marine Ecology Progress Series, 353, 255–264. URL: https://www.int-res.com/abstracts/meps/v353/p255-264/.L.
Hansen, M.C., Potapov, P.V., Moore, R., Hancher, M., Turubanova, S.A., Tyukavina, A., Thau, D., Stehman, S.V., Goetz, S.J., Loveland, T.R., Kommareddy, A., Egorov, A., Chini, L., Justice, C.O., Townshend, J.R.G., 2013. High-resolution global maps of 21st-century forest cover change. Science 342, 850–853.
Hermes, J.C., Reason, C.J.C., 2008. Annual cycle of the South Indian Ocean (Seychelles-Chagos) thermocline ridge in a regional ocean model. Journal of Geophysical Research: Oceans, 113. URL: https://onlinelibrary.wiley.com/doi/abs/10.1029/2007JC004363. _eprint: https://onlinelibrary.wiley.com/doi/pdf/10.1029/2007JC004363.
Hewitt, H.T., Roberts, M., Mathiot, P., Biastoch, A., Blockley, E., Chassignet, E.P., Fox-Kemper, B., Hyder, P., Marshall, D.P., Popova, E., Treguier, A.-M., Zanna, L., Yool, A., Yu, Y., Beadling, R., Bell, M., Kuhlbrodt, T., Arsouze, T., Bellucci, A., Castruccio, F., Gan, B., Putrasahan, D., Roberts, C.D., Van Roekel, L., Zhang, Q., 2020. Resolving and Parameterising the Ocean Mesoscale in Earth System Models. Curr. Clim. Change Rep. 6, 137–152. https://doi.org/10.1007/s40641-020-00164-w.
Hinojosa, I.A., Rivadeneira, M.M., Thiel, M., 2011. Temporal and spatial distribution of floating objects in coastal waters of central–southern Chile and Patagonian fjords. Continental Shelf Research, 31, 172–186. L.
Huret, M., Petitgas, P., Woillez, M., 2010. Dispersal kernels and their drivers captured with a hydrodynamic model and spatial indices: A case study on anchovy (Engraulis encrasicolus) early life stages in the Bay of Biscay. Prog. Oceanogr. 87, 6–17. URL: http://www.sciencedirect.com/science/article/pii/S0079661110001357. L.
Imzilen, T., Chassot, E., Barde, J., Demarcq, H., Maufroy, A., Roa-Pascuali, L., Ternon, J.-F., Lett, C., 2019. Fish aggregating devices drift like oceanographic drifters in the near-surface currents of the Atlantic and Indian Oceans. Progress in Oceanography, 171, 108–127. URL: https://linkinghub.elsevier.com/retrieve/pii/S0079661118301563 NL.
Institute, F.M., 2018 IHO Sea Areas, version 3.
IOTC (2022a) Executive Summary Bigeye Tuna (2022). Tech. rep., Indian Ocean Tuna Commission. URL: https://iotc.org/sites/default/files/documents/2022/11/IOTC-2022-SC25-ES02_BET_E.pdf.
IOTC (2022b) Executive Summary Yellowfin Tuna (2022). Tech. rep., Indian Ocean Tuna Commission. URL: https://iotc.org/sites/default/files/documents/2022/11/IOTC-2022-SC25-ES04_YFT_E.pdf.
IOTC (2022c) Overview of Indian Ocean tropical tuna fisheries. Working Party on Tropical Tunas: Data Preparatory Meeting IOTC-2022-WPTT24(DP)-07-TROPICAL, Indian Ocean Tuna Commission, Online. URL: https://iotc.org/documents/WPTT/24DP/07-01.
IOTC (2022d) Review of data on Drifting Fish Aggregating Devices. IOTC ad hoc Working Group on FADs (WGFAD) IOTC-2022-WGFAD03-03-Rev 2, Indian Ocean Tuna Commission, Online. URL: https://iotc.org/meetings/3rd-iotc-ad-hoc-working-group-fads-wgfad03.
IPBES (2018) The IPBES assessment report on land degradation and restoration. Tech. rep., Zenodo. URL: https://zenodo.org/record/3237393.
IPBES (2019) Global assessment report on biodiversity and ecosystem services of the Intergovernmental Science-Policy Platform on Biodiversity and Ecosystem Services. Tech. rep., Zenodo. URL: https://zenodo.org/record/6417333.
IPBES (2022) Thematic assessment of the sustainable use of wild species of the Intergovernmental Science-Policy Platform on Biodiversity and Ecosystem Services. Bonn, Germany: IPBES secretariat. URL: https://zenodo.org/record/7755805.
Jauharee, A.R., Capello, M., Simier, M., Forget, F., Adam, M.S., Dagorn, L., 2021. Tuna behaviour at anchored FADs inferred from Local Ecological Knowledge (LEK) of pole-and-line tuna fishers in the Maldives. PLOS ONE 16, e0254617. URL: https://dx.plos.org/10.1371/journal.pone.0254617.
Krajick, K., 2001. Defending Deadwood. Science 293, 1579–1581. URL: https://science.sciencemag.org/content/293/5535/1579/tab-pdf. L.
Lett, C., Verley, P., Mullon, C., Parada, C., Brochier, T., Penven, P., Blanke, B., 2008. A Lagrangian tool for modelling ichthyoplankton dynamics. Environmental Modelling & Software, 23, 1210–1214. URL: https://linkinghub.elsevier.com/retrieve/pii/S136481520800025X L.
Linke, S., Lehner, B., Ouellet Dallaire, C., Ariwi, J., Grill, G., Anand, M., Beames, P., Burchard-Levine, V., Maxwell, S., Moidu, H., Tan, F. and Thieme, M. (2019) Global hydro-environmental sub-basin and river reach characteristics at high spatial resolution. Scientific Data, 6, 283. URL: https://www.nature.com/articles/s41597-019-0300-6. Bandiera_abtest: a Cc_license_type: cc_publicdomain Cg_type: Nature Research Journals Number: 1 Primary_atype: Research Publisher: Nature Publishing Group Subject_term: Freshwater ecology;Hydrology Subject_term_id: freshwater-ecology;hydrology.
Macura, B., Byström, P., Airoldi, L., Eriksson, B.K., Rudstam, L., Støttrup, J.G., 2019. Impact of structural habitat modifications in coastal temperate systems on fish recruitment: a systematic review. Environ. Evid. 8, 14. https://doi.org/10.1186/s13750-019-0157-3.
Madec, G., 2016. the NEMO team: NEMO ocean engine. Note du Pôle de modélisation, Institut Pierre-Simon Laplace (IPSL). France 27, 1288–1619.
Marsac, F., Fonteneau, A. and Ménard, F. (2000) Drifting FADs used in tuna fisheries: an ecological trap? Pêche Thonière et Dispositifs de Concentration de Poissons, 28, 537–552. L.
Maufroy, A., Kaplan, D.M., Bez, N., De Molina, A.D., Murua, H., Floch, L., Chassot, E., 2017. Massive increase in the use of drifting Fish Aggregating Devices (dFADs) by tropical tuna purse seine fisheries in the Atlantic and Indian oceans. ICES J. Mar. Sci. 74, 215–225. URL: https://academic.oup.com/icesjms/article/74/1/215/2418180. L.
Mendenhall, E., 2018. Oceans of plastic: a research agenda to propel policy development. Mar. Policy 96, 291–298. URL: https://www.sciencedirect.com/science/article/pii/S0308597X18302902.
Merino, G., Murua, H., Santiago, J., Arrizabalaga, H., Restrepo, V., 2020. Characterization, Communication, and Management of Uncertainty in Tuna Fisheries. Sustainability, 12, 8245. URL: https://www.mdpi.com/2071-1050/12/19/8245. L.
Moreno, G., Dagorn, L., Sancho, G., García, D. and Itano, D. (2007) Using local ecological knowledge (LEK) to provide insight on the tuna purse seine fleets of the Indian Ocean useful for management. Aquatic Living Resources, 20, 367–376. URL: https://www.cambridge.org/core/journals/aquatic-living-resources/article/abs/using-local-ecological-knowledge-lek-to-provide-insight-on-the-tuna-purse-seine-fleets-of-the-indian-ocean-useful-for-management/CF24395D3C928AD42C106427194608BA. Publisher: EDP Sciences.
Nakamae, A., 1991. Artificial reef projects in Japan. Colombo, Sri Lanka.
Neumann, H., Diekmann, R., Kröncke, I., 2016. Functional composition of epifauna in the south-eastern North Sea in relation to habitat characteristics and fishing effort. Estuar. Coast. Shelf Sci. 169, 182–194. URL: https://linkinghub.elsevier.com/retrieve/pii/S0272771415301682.
Oppian (200 AD) Halieutica, vol. 4. London: Loeb Classical Library, London, Heinemann, 1963. URL: https://penelope.uchicago.edu/Thayer/E/Roman/Texts/Oppian/Halieutica/4*.html#404.
Pendrill, F., Gardner, T.A., Meyfroidt, P., Persson, U.M., Adams, J., Azevedo, T., Bastos Lima, M.G., Baumann, M., Curtis, P.G., De Sy, V., Garrett, R., Godar, J., Goldman, E. D., Hansen, M.C., Heilmayr, R., Herold, M., Kuemmerle, T., Lathuillière, M.J., Ribeiro, V., Tyukavina, A., Weisse, M.J. and West, C. (2022) Disentangling the numbers behind agriculture-driven tropical deforestation. Science, 377, eabm9267. URL: https://www.science.org/doi/abs/10.1126/science.abm9267. Publisher: American Association for the Advancement of Science.

Penduff, T., Barnier, B., Terray, L., Bessières, L., Sérazin, G., Gregorio, S., Brankart, J.M., Moine, M.P., Molines, J.M., Brasseur, P., 2014. Ensembles of eddying ocean simulations for climate. CLIVAR Exchanges, Special Issue on High Resolution Ocean Climate Modelling, p. 19.

Phillips, J.S., Escalle, L., Pilling, G., Gupta, A.S., Sebille, E.v., 2019. Regional connectivity and spatial densities of drifting fish aggregating devices, simulated from fishing events in the Western and Central Pacific Ocean. Environ. Res. Commun. 1, 055001. URL: https://iopscience.iop.org/article/10.1088/2515-7620/ab21e9. L.

Pineda, J., Hare, J. and Sponaugle, S. (2007) Larval Transport and Dispersal in the Coastal Ocean and Consequences for Population Connectivity. Oceanography, 20, 22–39. URL: https://tos.org/oceanography/article/larval-transport-and-dispersal-in-the-coastal-ocean-and-consequences-for-po. L.

Pons, M., Kaplan, D., Moreno, G., Escalle, L., Abascal, F., Hall, M., Restrepo, V. and Hilborn, R. (2023) Benefits, concerns, and solutions of fishing for tunas with drifting fish aggregation devices. Fish and Fisheries, 24, 979–1002. URL: https://onlinelibrary.wiley.com/doi/abs/10.1111/faf.12780. _eprint: https://onlinelibrary.wiley.com/doi/pdf/10.1111/faf.12780.

Pérez, G., Dagorn, L., Deneubourg, J.-L., Forget, F., Filmalter, J.D., Holland, K., Itano, D., Adam, S., Jauharee, R., Beeharry, S.P., Capello, M., 2020. Effects of habitat modifications on the movement behavior of animals: the case study of Fish Aggregating Devices (FADs) and tropical tunas. Movement Ecol. 8, 47. https://doi.org/10.1186/s40462-020-00230-w.

Robert, M., Dagorn, L., Bodin, N., Pernet, F., Arsenault-Pernet, E.-J., Deneubourg, J.-L., 2014. Comparison of condition factors of skipjack tuna (Katsuwonus pelamis) associated or not with floating objects in an area known to be naturally enriched with logs. Can. J. Fish. Aquat. Sci. 71, 472–478. URL: https://cdnsciencepub.com/doi/abs/10.1139/cjfas-2013-0389. L.

Russell, M.B., Woodall, C.W., D'Amato, A.W., Fraver, S. and Bradford, J.B. (2014) Technical Note: Linking climate change and downed woody debris decomposition across forests of the eastern United States. Biogeosciences, 11, 6417–6425. URL: https://bg.copernicus.org/articles/11/6417/2014/. Publisher: Copernicus GmbH.

Saji, N.H., Goswami, B.N., Vinayachandran, P.N. and Yamagata, T. (1999) A dipole mode in the tropical Indian Ocean. Nature, 401, 360–363. Publisher: Nature Publishing Group UK London.

Schaefer, K.M., Fuller, D.W., Hampton, J., Caillot, S., Leroy, B. and Itano, D. (2015) Movements, dispersion, and mixing of bigeye tuna (Thunnus obesus) tagged and released in the equatorial Central Pacific Ocean, with conventional and archival tags. Fisheries research, 161, 336–355. Publisher: Elsevier.

Schott, F.A., Xie, S.-P., McCreary, J.P., 2009. Indian Ocean circulation and climate variability. Rev. Geophys. 47, RG1002. URL: http://doi.wiley.com/10.1029/2007RG000245.

Sempo, G., Dagorn, L., Robert, M. and Deneubourg, J.-L. (2013) Impact of increasing deployment of artificial floating objects on the spatial distribution of social fish species. Journal of Applied Ecology, 50, 1081–1092. URL: http://doi.wiley.com/10.1111/1365-2664.12140. L.

Siegel, D., Kinlan, B., Gaylord, B. and Gaines, S. (2003) Lagrangian descriptions of marine larval dispersion. Marine Ecology Progress Series, 260, 83–96. URL: http://www.int-res.com/abstracts/meps/v260/p83-96/. L.

Song, L., Shen, H., 2022. An integrated scheme for the management of drifting fish aggregating devices in tuna purse seine fisheries. Fisheries Management and Ecology, 30, 56–69. URL: https://onlinelibrary.wiley.com/doi/abs/10.1111/fme.12600. _eprint: https://onlinelibrary.wiley.com/doi/pdf/10.1111/fme.12600.

Soria, M., Dagorn, L., Potin, G. and Fréon, P. (2009) First field-based experiment supporting the meeting point hypothesis for schooling in pelagic fish. Animal Behaviour, 78, 1441–1446. URL: https://linkinghub.elsevier.com/retrieve/pii/S0003347209004400. L.

Stelfox, M., Lett, C., Reid, G., Souch, G. and Sweet, M. (2020) Minimum drift times infer trajectories of ghost nets found in the Maldives. Marine Pollution Bulletin, 154, 111037. URL: https://linkinghub.elsevier.com/retrieve/pii/S0025326X20301557. L.

Van der Stocken, T., Carroll, D., Menemenlis, D., Simard, M., Koedam, N., 2019. Global-scale dispersal and connectivity in mangroves. In: Proc. Nat. Acad. Sci., 116, pp. 915–922. URL: http://www.pnas.org/lookup/doi/10.1073/pnas.1812470116. L.

Swearer, S.E., Morris, R.L., Barrett, L.T., Sievers, M., Dempster, T. and Hale, R. (2021) An overview of ecological traps in marine ecosystems. Frontiers in Ecology and the Environment, 19, 234–242. URL: https://onlinelibrary.wiley.com/doi/10.1002/fee.2322. L.

Taquet, M. (2013) Fish aggregating devices (FADs): good or bad fishing tools? A question of scale and knowledge. Aquatic Living Resources, 26, 25–35. URL: https://www.cambridge.org/core/journals/aquatic-living-resources/article/abs/fish-aggregating-devices-fads-good-or-bad-fishing-tools-a-question-of-scale-and-knowledge/65648C14CCA9522D327E8A33627455A8. L.

Teo, H.C., Tan, N.H.L., Zheng, Q., Lim, A.J.Y., Sreekar, R., Chen, X., Zhou, Y., Sarira, T. V., De Alban, J.D.T., Tang, H., Friess, D.A. and Koh, L.P. (2023) Uncertainties in deforestation emission baseline methodologies and implications for carbon markets. Nature Communications, 14, 8277. URL: https://www.nature.com/articles/s41467-023-44127-9. Publisher: Nature Publishing Group.

Thiel, M., Gutow, L., 2005. The ecology of rafting in the marine environment. I. The floating substrata. In: Gibson, R.N., Atkinson, R.J.A., Gordon, J.D.M. (Eds.), Oceanography and Marine Biology: an annual review, vol. 42. Crc press edn L, pp. 181–264.

Tolotti, M., Guillotreau, P., Forget, F., Capello, M. and Dagorn, L. (2022) Unintended effects of single-species fisheries management. Environment, Development and Sustainability. URL: doi: 10.1007/s10668-022-02432-1.

Van Sebille, E., Griffies, S.M., Abernathey, R., Adams, T.P., Berloff, P., Biastoch, A., Blanke, B., Chassignet, E.P., Cheng, Y. and Cotter, C.J. (2018) Lagrangian ocean analysis: Fundamentals and practices. Ocean Modelling, 121, 49–75. NL.

Van Sebille, E., Wilcox, C., Lebreton, L., Maximenko, N., Hardesty, B.D., Van Franeker, J. A., Eriksen, M., Siegel, D., Galgani, F. and Law, K.L. (2015) A global inventory of small floating plastic debris. Environmental Research Letters, 10, 124006. L.

Viatte, C., Clerbaux, C., Maes, C., Daniel, P., Garello, R., Safieddine, S., Ardhuin, F., 2020. Air Pollution and Sea Pollution Seen from Space. Surv. Geophys. 41, 1583–1609. URL: http://link.springer.com/10.1007/s10712-020-09599-0.

Wain, G., Guéry, L., Kaplan, D.M., Gaertner, D., 2021. Quantifying the increase in fishing efficiency due to the use of drifting FADs equipped with echosounders in tropical tuna purse seine fisheries. ICES J. Mar. Sci. 78, 235–245. https://doi.org/10.1093/icesjms/fsaa216.

Zhang, J., Wang, C., 2023. Zonal current structure of the Indian Ocean in CMIP6 models. Deep Sea Res. Part II 208, 105260. URL: https://www.sciencedirect.com/science/article/pii/S0967064523000103.